Structured Radio Wave Generation for Target State Estimation via Satellite Formations

Miki Yonehara, Makoto Ito, Hisatoshi Kimura, Keigo Nakamura,
Yosuke Tanabe, Tsukasa Funane, and Koichi Watanabe
Next Research, Research & Development Group, Hitahi, Ltd., Japan

***Abstract*—This paper proposes a formation-flying synthetic aperture radar (SAR) architecture in which multiple transmit-receive satellites form a sparse circular constellation and synthesize an orbital angular momentum (OAM)-like wavefront without dedicated OAM hardware. The central idea is to treat the grating lobes inherent to sparse arrays not as artifacts to be fully suppressed, but as additional spatially separated beams that can be incorporated into observation design. To analyze this architecture, we model the constellation as a sparse uniform circular array and derive its array factor by using a Jacobi-Anger expansion. We then validate the analytical representation against direct array-factor calculation and show that it accurately reproduces the main-lobe and first-grating-lobe structure relevant to mission design. On that basis, we derive three practical design guidelines. First, stable vortex-like phase topology requires an even number of satellites; odd-N configurations cause phase-topology collapse in the grating-lobe region. Second, L-band operation is more practical than shorter-wavelength bands for large sparse formations because it preserves usable beamwidth and separability between the main lobe and grating lobes. Third, grating-lobe locations are analytically predictable, which enables their use as designable observation resources rather than uncontrolled interference. These results define a design basis for a distributed aperture SAR architecture in which formation geometry, wavefront synthesis, and signal processing are treated in an integrated manner. The proposed approach targets wide-area, high-resolution, multi-observable sensing in a single pass with small-satellite constellations.**

***Index Terms*—formation flying SAR, distributed aperture SAR, orbital angular momentum, grating lobe, sparse UCA, small satellite constellation**

I. Introduction

Achieving both high spatial resolution and wide-swath coverage remains a central challenge in synthetic aperture radar (SAR) system design. Monostatic SAR implemented on a single satellite can produce high-quality imagery, but a fundamental trade-off persists among antenna aperture, swath width, and the amount of information that can be acquired in one pass [1], [2]. Once wide coverage, high resolution, three-dimensional observability, and moving-target observability are all required simultaneously, a single-platform architecture becomes increasingly difficult to scale. This limitation has motivated the progressive distribution of SAR functions across multiple spacecraft.

Formation-flying SAR has evolved in stages to address this limitation. TanDEM-X established the feasibility of formation-flying SAR by demonstrating single-pass interferometric observation with two homogeneous transmit-receive satellites while maintaining precise long-term relative geometry in orbit [3], [4]. More recent architectures, including Harmony and PIESAT, extend geometric diversity and multi-baseline sensing by combining one illuminator with multiple receive-only satellites [5]–[7]. In parallel, multiple transmit-receive constellations such as SATURN point toward still higher sensing degrees of freedom through more fully distributed transmission and reception [8], [9]. The natural next question is whether the formation can serve not only as a distributed sensing baseline, but also as a wave-synthesis aperture.

This paper investigates an orbital angular momentum (OAM) SAR constellation as a further step in distributed aperture SAR, where the formation itself acts as a wave-synthesis aperture. Here, the term "structured radio wave" refers to a radio field whose phase and spatial wavefront are intentionally structured [10]–[13]. In this paper, it specifically denotes the OAM-like wavefront synthesized by formations of phase-coordinated conventional SAR satellites. When multiple transmit-receive satellites are phase-synchronized on a sparse circle, grating lobes, normally treated as unwanted responses, can instead be used as additional spatially separated beams. The contribution of this paper is therefore twofold: it validates an analytical model that links sparse-array geometry to the resulting beam and phase structure, and it uses that model to derive practical design guidelines for grating-lobe-enabled observation. Specifically, we show that L-band operation is practical for large sparse formations, stable vortex-like phase topology requires an even number of satellites, and grating-lobe locations are predictable enough to be designed into the observation geometry.

II. Mission Concept and System Architecture

The proposed system places multiple transmit-receive satellites on a sparse circle so that the formation as a whole behaves as a large distributed aperture. A representative reference case is a six-satellite L-band constellation in low Earth orbit with a formation radius of several tens of meters. The resulting virtual aperture diameter can also reach several tens of meters, enabling angular directivity and spatial resolution that would be difficult to obtain from the physical antenna size of a single small satellite.

Corresponding author: Miki Yonehara (miki.yonehara.cs@hitachi.com).

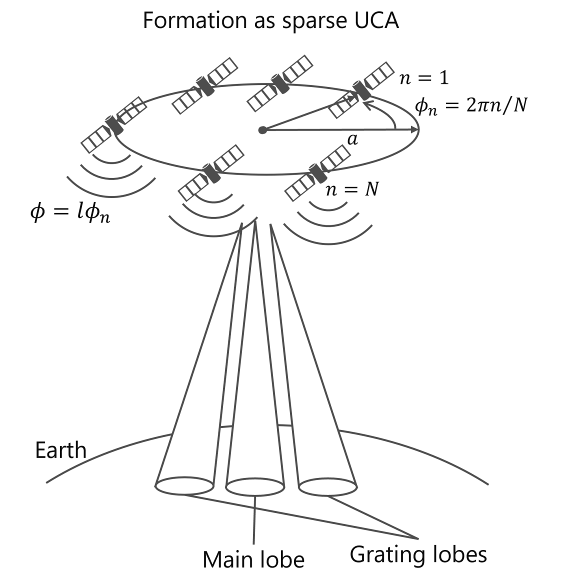

Fig. 1. Concept of the proposed formation-flying OAM-SAR constellation. Multiple transmit-receive satellites are arranged in a sparse circular formation, and phase-synchronized transmission synthesizes an OAM-like wavefront across the formation. The figure schematically shows the sharp main lobe together with surrounding grating-lobe beams, illustrating a single-pass multi-beam observation architecture.

TABLE I
REPRESENTATIVE DESIGN PARAMETERS OF THE PROPOSED SMALL-SATELLITE OAM-SAR CONSTELLATION

Item	Assumed value
Orbit altitude	Approximately 500 km
Operating band	L-band
Number of satellites	$N = 6$
Formation radius	$a \approx 30$ m
Virtual aperture	$D \approx 60$ m

No satellite requires dedicated OAM hardware. Instead, the constellation uses conventional plane-wave SAR payloads and synthesizes the structured radio wave considered here as a vortex-like wavefront through coordinated phase control across the formation. The key idea is therefore not hardware specialization but spatial wavefront synthesis through the combination of formation geometry and phase-synchronized operation. In this sense, the concept extends distributed transmit-receive architectures toward a configuration in which the formation itself becomes the wave-synthesis aperture [14], [15].

The grating lobes produced by sparse spacing are the second defining feature. In conventional array design, they are undesirable because they create ambiguous responses. Here, by contrast, they are treated as additional spatially separated beams that may be exploited intentionally [16]. If both the sharp main lobe and several grating lobes can serve as observation channels, the trade-off between narrow footprint and wide-area sensing can be relaxed, enabling a multi-beam architecture that acquires information from multiple directions in a single pass.

III. Mathematical Framework of Sparse UCA

A. Analytical Decomposition of Sparse-UCA Array Factor

To evaluate the radiation characteristics of the proposed formation, we consider a sparse uniform circular array in which N satellites are equally spaced on a circle of radius a. When an azimuthal phase gradient corresponding to OAM mode index l is imposed across the satellites, the array factor in observation direction (θ, ϕ) is given by the superposition of the geometric phase and the imposed phase used to synthesize the desired wavefront. The resulting pattern is determined by formation radius, wavelength, number of satellites, and mode index, and is therefore naturally interpreted as a spatial mode structure containing the main lobe together with higher-order components.

Using the Jacobi-Anger expansion,

$$\exp(jz\cos\alpha) = \sum_{m=-\infty}^{\infty} j^m J_m(z) e^{jm\alpha}, \tag{1}$$

the array factor can be transformed into a superposition of cylindrical-wave components [14], [15]. After evaluating the element sum, only the modes with $m = l + qN$ remain, yielding

$$\begin{aligned} AF(\theta,\phi) &= Nj^l J_l(ka\sin\theta) e^{jl\phi} \\ &\quad + N\sum_{q\neq 0} j^{l+qN} J_{l+qN}(ka\sin\theta) e^{j(l+qN)\phi}. \end{aligned} \tag{2}$$

The first term corresponds to the desired main lobe, and the terms with $q \neq 0$ correspond to grating-lobe components. Grating lobes therefore do not arise accidentally from implementation errors; they are an inherent consequence of spatial sampling in sparse arrays [16]. The key design question is thus not how to eliminate grating lobes completely, but under what conditions the main lobe and grating lobes remain spatially separable and the associated phase topology remains stable.

B. Numerical Validation of the Jacobi-Anger Representation

To validate the analytical representation used in the following section, we compare it with the original discrete element-sum expression,

$$AF(\theta,\phi) = \sum_{n=1}^{N} \exp\left\{ jl\phi_n + jka\sin\theta\cos(\phi-\phi_n) \right\}, \tag{3}$$

which serves as the reference calculation for the sparse circular formation. Figure 2 compares this direct evaluation with the Jacobi-Anger representation using a sufficiently wide summation range in q. The amplitude and phase maps, together with the representative cuts, show close agreement in the main-lobe region and in the first grating-lobe region. This confirms that the analytical mode decomposition reproduces not only the dominant beam direction but also the phase structure relevant to grating-lobe-enabled observation.

The truncation behavior of the expansion is also informative. Retaining only the $q = 0$ term is sufficient to describe the main-lobe component, but it does not reproduce the grating-lobe region. Including the $q = \pm 1$ terms captures the first

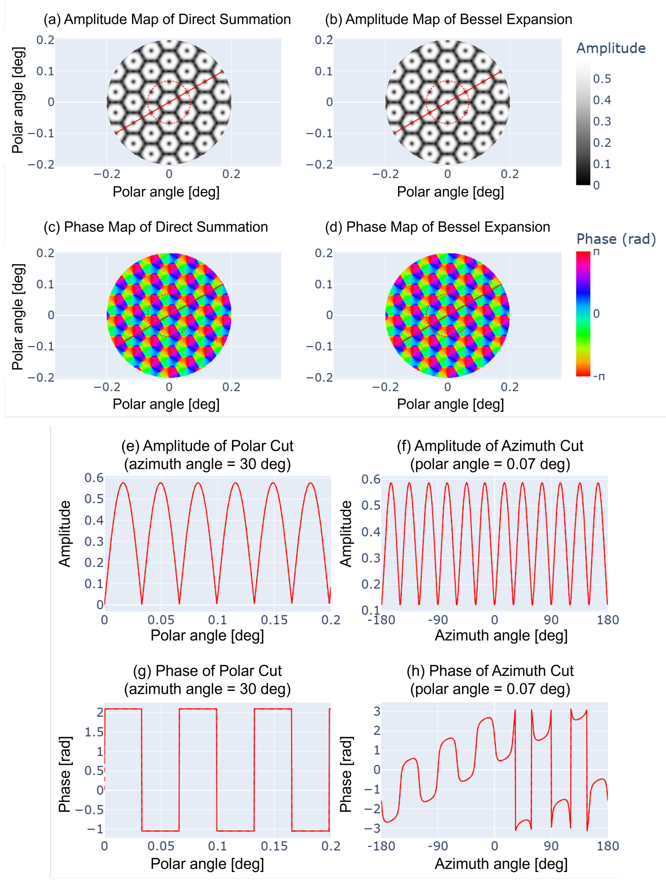

Fig. 2. Comparison between direct array-factor calculation and the analytical result obtained from the Jacobi-Anger expansion for a sparse UCA. Subplots (a)-(d) show the two-dimensional maps: (a) amplitude from direct summation, (b) amplitude from the Bessel expansion, (c) phase from direct summation, and (d) phase from the Bessel expansion. Subplots (e)-(h) show the corresponding cuts: (e) polar-cut amplitude, (f) azimuth-cut amplitude, (g) polar-cut phase, and (h) azimuth-cut phase. The figure confirms close agreement in the positions of the main lobe and dominant grating-lobe components as well as in their phase structure.

grating lobe accurately, while higher-order terms mainly affect outer lobes beyond the scope of the present design discussion. This is important because the design rules in Section IV focus on the main lobe and the first grating lobe. The validation therefore supports the use of the analytical decomposition as a practical and sufficiently accurate model for deriving the proposed engineering guidelines.

IV. Design Guidelines for Constellation OAM-SAR

A. Scale Law and Frequency Selection

For large sparse formations implemented with small satellites, L-band is more practical than shorter-wavelength bands. The spatial pattern of a sparse UCA is governed strongly by electrical size a/λ, and once the formation radius reaches several tens of meters, shorter wavelengths make the main lobe excessively narrow and push the grating lobes closer to it [14], [15], [17]. For example, with $N = 6$ and $a = 30$ m, the main-lobe width in X-band can shrink to roughly $0.03°$, while the first grating lobe appears around $0.055°$, making clean spatial separation extremely difficult. This is problematic not because high resolution is undesirable, but because it undermines the idea of using grating lobes as independently useful beams.

By contrast, in L-band, the Bessel-function argument in (2), $z = ka \sin\theta = (2\pi a/\lambda)\sin\theta$, varies more moderately. For the same formation radius, the main lobe and the first grating lobe therefore retain meaningful angular separation. If the element spacing is approximated as $d \approx 2\pi a/N$, the first grating lobe appears approximately when $\sin\theta \gtrsim \lambda/d$. Under the same representative parameters, the main-lobe width is about $0.22°$ and the first grating lobe appears around $0.42°$, leaving a usable separation region for observation design. Thus, in a large sparse OAM-SAR constellation, operating frequency must be chosen not only for nominal resolution but also for separability between the main lobe and the grating lobes. From this perspective, L-band is a practical engineering choice.

At first sight, X-band may appear to be the more natural choice because many low-Earth-orbit small-satellite SAR constellations operate in that band. For the present concept, however, beamwidth rather than heritage is the limiting consideration. With realistic formation radii of several tens of meters, X-band makes the main beam so narrow that the illuminated ground swath becomes too limited for the intended observation concept, and the usable separation margin between the main lobe and grating lobes is correspondingly reduced. One possible countermeasure would be to move to a higher orbit so that the narrow beam maps to a more practical ground swath, but this direction raises the power burden and overall mission difficulty. For this reason, the proposed architecture treats L-band as the more practical baseline for small-satellite formation flying.

In practical mission design, frequency selection therefore determines not only nominal resolution but also ground footprint, grating-lobe separability, and the orbit-power trade space. Operating band, formation radius, and mission geometry must consequently be chosen together rather than optimized independently.

B. Phase Topology and Parity of N

An even number of satellites is important for stable vortex-like phase formation. In the Jacobi-Anger-based decomposition, the relative phase between the main lobe and the dominant grating-lobe component is governed by the factor $j^{\pm N}$, so the parity of N directly controls the phase topology. When N is odd, the dominant main-lobe and first-grating-lobe components tend to become orthogonal in the complex plane, producing standing-wave-like interference in azimuth. As a result, the intended smooth vortex-like phase structure collapses into a mosaic-like pattern [14], [15].

Considering only the coefficient ratio between the main-lobe term and the dominant first-grating-lobe term in (2), the relative phase is

$$\frac{A_{GL}}{A_{ML}} = \frac{j^{l\pm N}}{j^{l}} = j^{\pm N}. \tag{4}$$

If N is even, then $j^{\pm N} = \pm 1$ and the main-lobe and grating-lobe components interfere along the same axis in the complex plane. If N is odd, then $j^{\pm N} = \pm j$ and the two components tend to become orthogonal. The parity of N therefore directly determines whether the phase topology remains coherent or breaks down.

When N is even, the relative phase alignment between the main lobe and grating lobes is much more favorable for maintaining a continuous rotating phase structure. Even-N selection is therefore not merely aesthetic; it is a practical condition for treating the synthesized phase topology as a stable design variable. For small-satellite constellations, an even-N circular formation with about six satellites is a natural reference point because it balances geometric simplicity, virtual-aperture size, and phase stability.

From an engineering standpoint, even-N should therefore be treated as a design constraint rather than as a preferred option. This makes six-satellite-class formations particularly attractive because they offer a practical compromise among topology stability, virtual-aperture scale, and operational complexity.

Figure 3 shows the odd-N case using both two-dimensional maps and representative cuts. The figure confirms that the grating-lobe region exhibits not only mosaic-like phase collapse in two dimensions but also step-like phase discontinuities in one-dimensional cuts. The problem with odd N is therefore not only visual irregularity, but loss of the phase topology itself.

C. Spatial Configuration of Grating Lobes

The spatial configuration of grating lobes is analytically predictable and can therefore be treated not only as a constraint but also as a design variable. Extracting the $q = \pm 1$ terms that dominate the first grating lobe from (2), we obtain, under the even-N condition,

$$AF_{GL1}(\theta, \phi) \approx C e^{jl\phi} \big[J_{l+N}(z) e^{jN\phi} + J_{l-N}(z) e^{-jN\phi} \big], \quad z = ka \sin\theta. \tag{5}$$

Hence, the ring location of the first grating lobe is determined by the balance condition

$$J_{N+l}(z_{\text{ring}}) = J_{N-l}(z_{\text{ring}}), \qquad \theta_{\text{ring}} = \arcsin\left(\frac{z_{\text{ring}}}{ka}\right). \tag{6}$$

Along this ring, the azimuthal envelope follows $|\cos(N\phi)|$ or $|\sin(N\phi)|$, which means that $2N$ peaks and $2N$ nulls appear regularly in azimuth [14], [17], [18].

This result implies that grating lobes should not be treated merely as accidental sidelobe artifacts. Once their locations are predicted analytically, they can be incorporated into the observation design as beam resources. The choice of satellite count and formation radius therefore determines not only the main-lobe properties but also the additional beams generated around it. The proposed architecture uses this predictability to define a multi-beam observation concept that includes both the main lobe and multiple grating lobes.

This predictability provides more than a qualitative explanation of the beam pattern; it introduces a usable degree of freedom for observation geometry. The ring radius of the first grating lobe determines where additional beams appear, and the associated $2N$ azimuthal peaks and nulls indicate how observation resources can be distributed in angle. The choice of satellite count N and formation radius a therefore controls not only main-lobe gain and virtual-aperture size but also beam separability, azimuthal beam placement, and the diversity of directions that can be sensed in a single pass. In the proposed architecture, this geometric predictability is the key condition that allows grating lobes to be treated as observation channels rather than as unwanted interference.

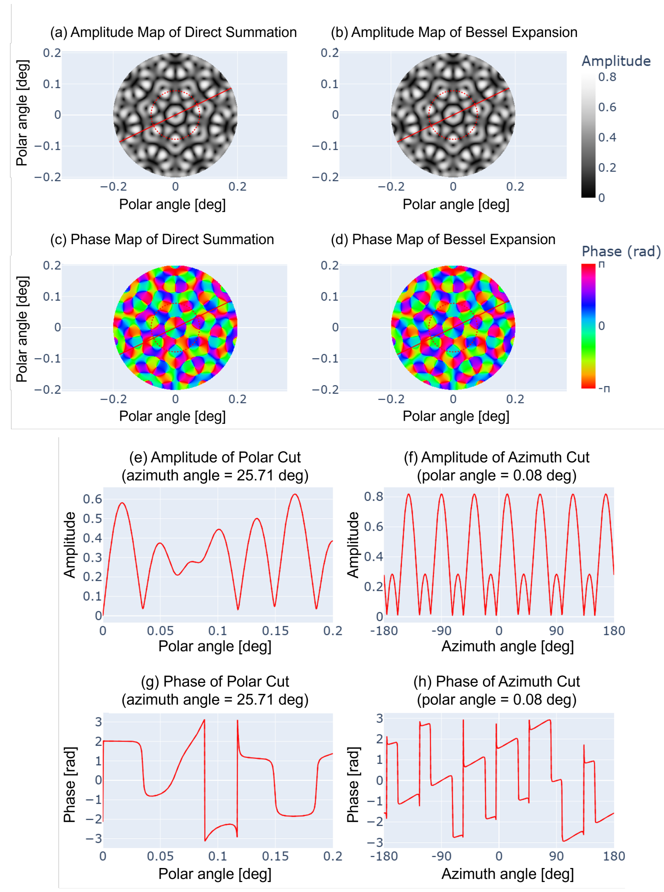

Fig. 3. Phase-topology collapse in the odd-N case. Subplots (a)-(d) show the two-dimensional maps: (a) amplitude from direct summation, (b) amplitude from the Bessel expansion, (c) phase from direct summation, and (d) phase from the Bessel expansion. Subplots (e)-(h) show the corresponding cuts: (e) polar-cut amplitude, (f) azimuth-cut amplitude, (g) polar-cut phase, and (h) azimuth-cut phase. In the grating-lobe region, the phase collapses into a mosaic-like pattern, and the cuts show step-like phase jumps. This confirms that stable OAM-like wavefront formation strongly favors even-N selection.

V. Operational Feasibility

The value of the proposed approach lies in combining a large virtual aperture with grating-lobe-enabled multi-beam observation so that several sensing benefits can be obtained in a single pass. If the virtual aperture sharpens the main lobe sufficiently, the system can target spatial resolution beyond the practical reach of conventional small-satellite SAR. If the surrounding grating lobes are also usable as independent beams, they can compensate for the narrow footprint of the main lobe and provide multiple observation channels simultaneously. In addition, the azimuth-dependent phase structure of the OAM-like wavefront suggests a path toward integrating wide-area coverage, high resolution, three-dimensional observability, and moving-target observability within a single-pass architecture. The proposed concept should therefore be viewed not merely as a resolution-enhancement scheme, but as an attempt to expand the observation mode itself through a small-satellite constellation.

Several implementation challenges must nevertheless be addressed before such a mission becomes practical. The first is relative navigation and phase synchronization. Position errors and oscillator mismatches directly degrade wavefront synthesis, but high-precision relative navigation and inter-satellite synchronization have already been demonstrated in formation-flying SAR missions [3], [4], [19]–[21]. The proposed concept assumes that these technologies can be combined with digital phase compensation so that requirements on physical position control and wavefront accuracy can be allocated across different design layers. The key point is not to hold every satellite at an ideal geometric point at all times, but to estimate and compensate relative errors well enough to preserve beam coherence during the observation interval.

The second challenge is grating-lobe signal separation. To use multiple additional beams as sensing resources, the corresponding echo components must be separated and interpreted reliably. This challenge is closely related to recent signal-processing advances in distributed SAR and multiple input multiple output (MIMO) SAR, including adaptive digital beamforming and blind source separation [9], [22]–[25]. In the present concept, analytical predictability of grating-lobe location is particularly important because it provides prior information to the separation stage. If likely peak positions and phase structures are known in advance, the additional beams can be treated not as uncontrolled interference but as model-based observation channels.

The third challenge is formation-maintenance cost. Maintaining a sparse formation with characteristic separations of several tens of meters over mission timescales raises propulsion and operational burdens. Here again, if part of the geometric imperfection can be absorbed by digital phase compensation, a more practical trade-off becomes available between fuel consumption and wavefront quality [19], [26]–[28]. It is also unnecessary to impose the same geometric tolerance at all times. Mode-dependent control strategies are possible: tighter control may be required only during high-resolution observation, whereas looser control may be acceptable when the priority is wide-area multi-beam sensing through grating-lobe utilization.

Feasibility also depends on whether these component technologies can be connected into a single observation chain rather than demonstrated in isolation. A plausible implementation path starts from formation flying that establishes relative position and time synchronization, proceeds to distributed phase calibration and wavefront synthesis across the constellation, and then uses analytically predicted grating-lobe locations as prior information for echo separation and image formation. From this viewpoint, the difficulty of the proposed architecture lies not only in its higher control demand, but in how consistently navigation, synchronization, wavefront compensation, and signal processing can be integrated into one mission system. If that integration is achieved, the architecture offers a route toward combining high resolution, broader effective coverage, and richer single-pass observability within a single formation-flying SAR concept.

TABLE II
CAPABILITY COMPARISON OF MONOSTATIC SAR, INSAR FORMATIONS, MIMO-SAR, AND THE PROPOSED OAM-SAR CONSTELLATION. SWATH: WIDE-SWATH CAPABILITY; RES.: SPATIAL RESOLUTION; 3D: SINGLE-PASS THREE-DIMENSIONAL OBSERVABILITY; VEL.: MOVING-TARGET VELOCITY OBSERVABILITY; CTRL.: FORMATION-CONTROL DEMAND.

Architecture	Swath	Res.	3D	Vel.	Ctrl.
Monostatic	High	Medium	Low	Low	Low
InSAR form.	Medium	Medium	High	Low	Medium
MIMO-SAR	High	High	Medium	Medium	High
Proposed	High	High	High	High	High

The proposed architecture should also be positioned against existing observation concepts. Conventional monostatic SAR remains effective for high-quality imaging, but its physical aperture directly couples resolution and swath width. Formation-flying InSAR extends the architecture to single-pass three-dimensional observation, yet the system still operates essentially with a shared beam and therefore does not remove the resolution-swath trade-off. MIMO-SAR offers a path toward simultaneous high resolution and wider coverage, but in wide continuous scenes it must preserve waveform orthogonality under difficult interference conditions [9], [22]. The present concept takes a different route: it relies on spatial mode structure and analytically predictable grating-lobe placement rather than waveform multiplexing alone, with the aim of combining high resolution, wide-area coverage, and richer single-pass observability within one formation architecture.

From this viewpoint, the proposed concept should not be interpreted as a fully mature mission definition, but as a next-step architecture whose feasibility can already be discussed within the current technology line of formation-flying SAR [5], [7], [8], [29]. Its novelty lies not in assuming an unrealistically perfect formation to generate an exotic wavefront, but in treating the analytically predictable main-lobe and grating-lobe structure as part of a mission architecture explicitly linked to navigation, synchronization, and signal processing. Table II compares monostatic SAR, InSAR formations, MIMO-SAR, and the proposed OAM-SAR constellation in terms of wide-swath capability, high resolution, single-pass 3D observability, velocity observability, and formation-control demand.

VI. CONCLUSION AND FUTURE WORK

This paper presented three practical design guidelines for a formation-flying OAM-SAR constellation: even-N selection, L-band operation, and analytically predictable grating-lobe placement. Together, these results provide a design basis for distributed aperture SAR architectures aimed at wide-area, high-resolution, multi-observable sensing in a single pass with small-satellite formations.

The next step is to convert these guidelines into an implementable observation chain. Priority topics include grating-lobe echo separation and image formation, distributed synchronization and calibration across multiple satellites, and wavefront-compensation methods that explicitly account for orbital distortion and synchronization error. A further task is end-to-end parameter optimization under realistic propagation and power constraints so that the trade-offs among orbit design, operating band, beam geometry, and observation performance can be evaluated at mission level.

References

[1] R. F. Hanssen, *InSAR Principles: Guidelines for SAR Interferometry Processing and Interpretation*, ser. ESA TM-19. European Space Agency, 2007.

[2] JAXA, "Advanced Land Observing Satellite-4 (ALOS-4) Press Kit," Online, 2024. [Online]. Available: https://fanfun.jaxa.jp/countdown/alos4-h3/files/alos-4_presskit_20240628.pdf

[3] G. Krieger, A. Moreira, H. Fiedler, I. Hajnsek, M. Werner, M. Younis, and M. Zink, "TanDEM-X: A Satellite Formation for High-Resolution SAR Interferometry," *IEEE Transactions on Geoscience and Remote Sensing*, vol. 45, no. 11, pp. 3317–3341, 2007. [Online]. Available: https://doi.org/10.1109/TGRS.2007.900693

[4] M. Zink, A. Moreira, I. Hajnsek, G. Krieger, M. Younis, and H. Fiedler, "TanDEM-X: The New Global DEM Takes Shape," *IEEE Geoscience and Remote Sensing Magazine*, vol. 2, no. 2, pp. 8–23, 2014. [Online]. Available: https://doi.org/10.1109/MGRS.2014.2318895

[5] A. Kääb, J. Mouginot, P. Prats-Iraola, E. Rignot, B. Rabus, A. Benedikter, H. Rott, T. Nagler, B. Rommen, and P. Lopez-Dekker, "Potential of the Bi-Static SAR Satellite Companion Mission Harmony for Land-Ice Observations," *Remote Sensing*, vol. 16, no. 16, p. 2918, 2024. [Online]. Available: https://www.mdpi.com/2072-4292/16/16/2918

[6] eoPortal, "Harmony Mission Summary," Online, 2024. [Online]. Available: https://www.eoportal.org/satellite-missions/harmony

[7] T. Zhang, Y. Qian, C. Li, J. Lu, J. Fu, Q. Guo, S. Guo, and Y. Wang, "Imaging and Interferometric Mapping Exploration for PIESAT-01: The World's First Four-Satellite "Cartwheel" Formation Constellation," *Atmosphere*, vol. 15, no. 6, p. 621, 2024. [Online]. Available: https://www.mdpi.com/2073-4433/15/6/621

[8] OHB Italia, "The SATURN Mission," Online, 2024. [Online]. Available: https://www.ohb-italia.it/the-saturn-mission/

[9] G. Krieger, "MIMO-SAR: Opportunities and Pitfalls," *IEEE Transactions on Geoscience and Remote Sensing*, vol. 52, no. 5, pp. 2628–2645, 2014. [Online]. Available: https://doi.org/10.1109/TGRS.2013.2261919

[10] Y. Tanabe, T. Funane, H. Kimura, M. Ito, S. Saito, and K. Watanabe, "Structured Radio Waves for Multiplex Communications and Radar Imaging," *Journal of Evolving Space Activities (JESA)*, 2026, accepted for publication.

[11] H. Kimura, Y. Tanabe, T. Funane, M. Ito, and K. Watanabe, "Study on Partial Detection of Orbital Angular Momentum in Radio Wave," *Journal of Evolving Space Activities (JESA)*, 2026, accepted for publication.

[12] Y. Tanabe, H. Kimura, M. Ito, K. Nakamura, T. Funane, S. Saito, K. Watanabe, M. Yonehara, K. Suzuki, Y. Takahashi, Y. Magara, S. Ikari, S. Nakasuka, T. Masuoka, A. Uematsu, S. Ozawa, and Y. Miyazaki, "Structured Radio Waves for Radar Imaging," in *AIAA SCITECH 2026 Forum*, 2026.

[13] M. Ito, Y. Tanabe, H. Kimura, K. Nakamura, M. Yonehara, T. Funane, S. Saito, K. Watanabe, K. Suzuki, Y. Takahashi, Y. Magara, S. Ikari, S. Nakasuka, T. Masuoka, S. Ozawa, A. Uematsu, and Y. Miyazaki, "Feasibility Study of Parabolic Reflector for Structured Radio Waves SAR in Small Satellites," in *AIAA SCITECH 2026 Forum*, 2026.

[14] M. Lin, Y. Gao, P. Liu, and J. Liu, "Theoretical Analyses and Design of Circular Array to Generate Orbital Angular Momentum," *IEEE Transactions on Antennas and Propagation*, vol. 65, no. 7, pp. 3510–3519, 2017. [Online]. Available: https://doi.org/10.1109/TAP.2017.2700160

[15] D. Liu, L. Gui, K. Chen, L. Lang, Z. Zhang, H. Chen, L. Liu, and T. Jiang, "Theoretical Analysis and Comparison of OAM Waves Generated by Three Kinds of Antenna Array," *Digital Communications and Networks*, vol. 7, no. 1, pp. 16–28, 2021.

[16] F. Ahmad and M. G. Amin, "Grating Lobe Suppression in Sparse Array Radar Imaging," *IEEE Transactions on Image Processing*, vol. 20, no. 4, pp. 1171–1174, 2011. [Online]. Available: https://doi.org/10.1109/TIP.2010.2090534

[17] P. Qi, D. Li, S. Zhu *et al.*, "Optimized Design Method for Multimodal Low-Coupling Orbital Angular Momentum Arrays for Radar Detection," *Journal of Radars*, 2025.

[18] N. Kou and S. Yu, "Low Sidelobe Orbital Angular Momentum Vortex Beams Based on Modified Bayliss Synthesis Method for Circular Array," *IEEE Antennas and Wireless Propagation Letters*, vol. 21, no. 5, pp. 968–972, 2022. [Online]. Available: https://doi.org/10.1109/LAWP.2022.3153392

[19] Q. Lin, S. Li, and W. Yu, "Review on Phase Synchronization Methods for Spaceborne Multistatic Synthetic Aperture Radar," *Sensors*, vol. 24, no. 10, p. 3122, 2024. [Online]. Available: https://www.mdpi.com/1424-8220/24/10/3122

[20] H. Kimura, Y. Tanabe, M. Ito, T. Funane, and K. Watanabe, "GNSS-free relative-distance measurement among multiple satellites using software-defined radio interferometry," *Journal of Evolving Space Activities (JESA)*, vol. 2, 2024. [Online]. Available: https://doi.org/10.57350/jesa.139

[21] R. Suzumoto, S. Ikari, N. Miyamura, and S. Nakasuka, "µm-class Control of Relative Position and Attitude for a Formation Flying Synthetic Aperture Telescope with Micro-satellites," *Transactions of the Japan Society for Aeronautical and Space Sciences*, vol. 64, no. 2, pp. 101–111, 2021. [Online]. Available: https://doi.org/10.2322/tjsass.64.101

[22] W. Peng, W. Wang, Y. Zhang, Y. Wei, and Z. Zhang, "A Novel MIMO SAR Scheme with Intra–Inter-Pulse Phase Coding and Azimuth–Elevation Joint Processing," *Remote Sensing*, vol. 17, no. 21, p. 3544, 2025. [Online]. Available: https://doi.org/10.3390/rs17213544

[23] X. Liu, J. Wang *et al.*, "A Novel Scheme for MIMO-SAR Systems Using Rotational Doppler Effect of OAM," *Sensors*, vol. 18, no. 10, p. 3511, 2018. [Online]. Available: https://doi.org/10.3390/s18103511

[24] "Echo Separation Method for Pitching Space-Time Coding Space-Borne SAR System," Chinese Patent Application, Publication No. CN114895260A, 2022. [Online]. Available: https://patents.google.com/patent/CN114895260A/en

[25] K. Yao and C. Liu, "A Novel Space–Time Coding Echo Separation Scheme with Orthogonal Frequency Division Multiplexing Chirp Waveforms for Multi-Input Multi-Output Synthetic Aperture Radar," *Sensors*, vol. 25, no. 6, p. 1717, 2025. [Online]. Available: https://www.mdpi.com/1424-8220/25/6/1717

[26] "Coded Synchronization for Bistatic SAR," European Patent Application, Publication No. EP3771921A1, 2021. [Online]. Available: https://patents.google.com/patent/EP3771921A1/en

[27] "Satellite Network Distributed Time Synchronization Control Method and System," Chinese Patent Application, Publication No. CN119030654A, 2024. [Online]. Available: https://patents.google.com/patent/CN119030654A/en

[28] K. Suda, S. Ikari, and S. Nakasuka, "Orbit Design for Earth-orbiting Formation Flying Satellites Aligned in a Straight Line toward a Celestial Target," *Transactions of the Japan Society for Aeronautical and Space Sciences*, vol. 68, no. 1, pp. 43–56, 2025. [Online]. Available: https://doi.org/10.2322/tjsass.68.43

[29] A. Renga, A. Gigantino, M. D. Graziano, A. Moccia, A. Fedele, and S. Natalucci, "Design Considerations and Performance Analysis for RODiO Distributed SAR Mission," *Acta Astronautica*, vol. 210, pp. 474–482, 2023. [Online]. Available: https://www.sciencedirect.com/science/article/pii/S0094576523001637